HNUE JOURNAL OF SCIENCE DOI: 10.18173/2354-1059.2021-0029
Natural Sciences 2021, Volume 66, Issue 2, pp. 66-74
This paper is available online at http://stdb.hnue.edu.vn

THE PRODUCTION OF SCALAR UNPARTICLE IN PAIR WITH PHOTON AND Z BOSON FROM $\mu^+\mu^-$ COLLISION IN UNPARTICLE PHYSICS

Le Nhu Thuc and Dao Thi Le Thuy
Faculty of Physics, Hanoi National University of Education

Abstract. This work aims to calculate the scalar unparticle (U_0) production in pair with photon and Z boson at $\mu^+\mu^-$ collision in unparticle physics perspective. The work shows that $\mu^+\mu^-$ collision process involving scalar unparticles with dimension $d_U < 2$ via the photon or Z boson exchange has been only done for s-channel while via muon (μ^-) exchange it has been done for *t* and *u*-channel. The cross-sections of the production of U_0 in the $\mu^+\mu^-$ collider when the μ^+, μ^- beams are unpolarized in unparticle physics were calculated in detail. The obvious dependence of differential cross-section (DCS) on the scattering angle (θ) and the cross-section (CS) on the center of mass-energy $(\sqrt{s})$ which is the available range of energy at the future high energy frontier muon collider in the Muon Accelerator Program (MAP) were evaluated respectively.

Keywords: scalar unparticle, muon, photon, Z boson, luminosity, DCS, CS.

1. Introduction

The way of dealing with conformal field theories had been proposed by Georgi [1, 2]. The correct propagator of a gauge invariant field is fixed up to normalization by the scaling dimension of the field. The phase space of the corresponding final state looks like that of a non-integer of particles, and so Georgi called them unparticles. The basic structure of unparticle physics was suggested by Georgi. This is the scale-invariant sector combined with the Standard Model (SM) through of an SM operator $\square_{\mathrm{SM}}$ and an unparticle operator $\square_{\mathrm{UV}}$ in which forms $\square_{\mathrm{UV}}\square_{\mathrm{SM}}$. The Lagrangian of the unparticle physics is as follows [3]:

$$L = \frac{c_n}{M^{d_{UV}+n-4}} \square_{\mathrm{UV}}\square_{\mathrm{SM}}, \tag{1.1}$$

Received February 18, 2021. Revised May 10, 2021. Accepted May 17, 2021.
Contact Le Nhu Thuc, e-mail address: thucln@hnue.edu.vn

where M is the energy scale characterizing the new physics, the operator$\square\square_{UV}$, and operator$\square\square_{SM}$ have dimensions d_{UV} and n respectively and c_n is a dimension-less constant. In the low energy effective theory, the Lagrangian has the form

$$L = c_n \frac{\Lambda_U^{d_{UV}-d_U}}{M^{d_{UV}+n-4}} \square_U \square_{SM}, \tag{1.2}$$

where the unparticle operator $\square_U$ with the dimension d_U. The d_U is a continuous parameter and is not necessarily bound to integer values. Unparticles would appear as fractional particles and for scalar unparticle operator, $1 \le d_U \le 2$. For vector and tensor unparticle operator of fermions, $3/2 \le d_U \le 5/2$) [4].

The collider phenomenology of unparticle physics and Feynman rules for the unparticle operators (scalar, vector, and tensor unparticle) with SM fields are presented in Ref. [5]. Subsequently, many studies on unparticles have studied constraining unparticle physics with cosmology and astrophysics [6], black holes [7-9], and super-conductors [10-12]. The data analysis by using Compact Muon Solenoid (CMS) detector at Large Hadron Collider (LHC) [13-16] is possible signature of the unparticle. In addition, unparticle production in collision processes was calculated by the Feynman rule [17-19].

In this paper, we calculate the $\mu^+\mu^-$ collision process involving scalar unparticles with the dimension $d_U < 2$ with the photon and Z boson exchange from *s*-channel while with μ^- exchange from *t* and *u*-channel. The cross-sections of the production of U_0 as well as its influence in the cross-section of the $\mu^+\mu^-$ collision when the μ^+, μ^- beams are unpolarized are also considered in detail. From the participation of unparticles, we evaluate the obvious dependence of the DCS on the θ and the CS on the $\sqrt{s}$ which is the available range of energy at the future high energy frontier muon collider in the MAP.

2. Content

2.1. The collision processes: $\mu^+\mu^- \to U_0\gamma$ and $\mu^+\mu^- \to U_0 Z$ in unparticle physics

The most important advantage of $\mu^+\mu^-$ collider is at energies above $2TeV$ with higher luminosities for an e^+e^- collider [20]. Therefore, the study of the production of unparticles in the $\mu^+\mu^-$ collider process may be tested experimentally.

The Feynman diagrams for the processes $\mu^+\mu^- \to U_0\gamma(Z)$ (with $\gamma(Z)$ stands for cases for photon or Z boson) are shown as

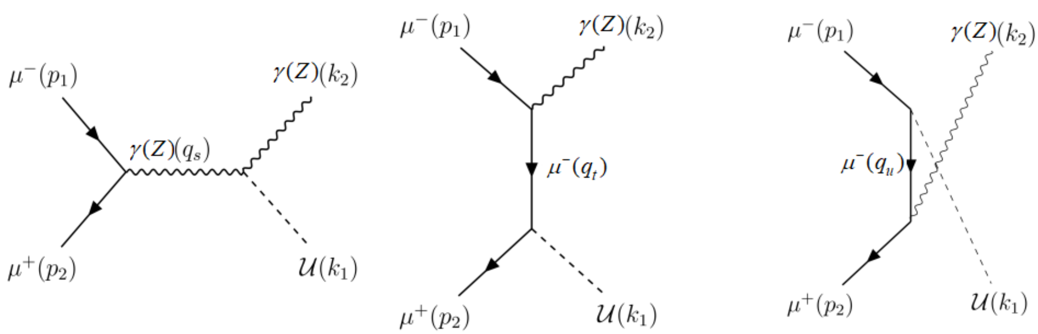

(a) s-channel (b) t-channel (c) u-channel

***Figure 1**. The Feynman diagrams for the processes* $\mu^+\mu^- \to U_0\gamma(Z)$

The scattering matrix elements of *s*, *t*, and *u* channels for each process $\mu^+\mu^- \to U_0\gamma$ and $\mu^+\mu^- \to U_0 Z$ were written respectively by applying the Feynman rule. For *s*-channel,

$$M_{s(\mu^+\mu^-\to U_0\gamma)} = \frac{4ie}{q_s^2}\frac{\lambda_0}{\Lambda_U^{d_u}}((\mathrm{q}_s\, k_2)\,\mathrm{g}^{\alpha\nu} - q_s^\alpha k_2^\nu)\varepsilon_\alpha^*(k_2)\times\bar{v}(\mathrm{p}_2,\mathrm{s}_2)\gamma_\nu u(p_1,s_1), \quad (2.1)$$

$$M_{s(\mu^+\mu^-\to U_0 Z)} = -\frac{ig}{C_\mathrm{w}(q_s^2-m_Z^2)}\frac{\lambda_0}{\Lambda_U^{d_u}}((\mathrm{q}_s\, k_2)\,\mathrm{g}^{\alpha\nu} - q_s^\alpha k_2^\nu)\varepsilon_\alpha^*(k_2)\left(g_{\nu\mu} - \frac{q_{s\nu}q_{s\mu}}{m_Z^2}\right)$$
$$\times\bar{v}(\mathrm{p}_2,\mathrm{s}_2)\gamma^\mu(\mathrm{v}_\mu - \mathrm{a}_\mu\gamma_5)u(p_1,s_1). \quad (2.2)$$

For *t*-channel,

$$M_{t(\mu^+\mu^-\to U_0\gamma)} = \frac{ie}{q_t^2-m_\mu^2}\frac{\lambda_0}{\Lambda_U^{d_u-1}}\varepsilon_\alpha^*(k_2)\bar{v}(\mathrm{p}_2,\mathrm{s}_2)\gamma^\alpha(\hat{\mathrm{q}}_t+\mathrm{m}_\mu)(1+i\gamma^5-\frac{i}{\Lambda_U}\hat{\mathrm{k}}_1)u(p_1,s_1), \quad (2.3)$$

$$M_{t(\mu^+\mu^-\to U_0 Z)} = \frac{-ig}{4C_\mathrm{w}(q_t^2-m_\mu^2)}\frac{\lambda_0}{\Lambda_U^{d_u-1}}\varepsilon_\alpha^*(k_2)$$
$$\times\bar{v}(\mathrm{p}_2,\mathrm{s}_2)(1+i\gamma^5-\frac{i}{\Lambda_U}\hat{\mathrm{k}}_1)(\hat{\mathrm{q}}_t+\mathrm{m}_\mu)\gamma^\alpha(\mathrm{v}_\mu-\mathrm{a}_\mu\gamma_5)u(p_1,s_1). \quad (2.4)$$

For *u*-channel,

$$M_{u(\mu^+\mu^-\to U_0\gamma)} = \frac{i\lambda_0}{\Lambda_U^{d_u-1}}\frac{e}{q_u^2-m_\mu^2}\varepsilon_\alpha^*(k_2)\bar{v}(\mathrm{p}_2,\mathrm{s}_2)(1+i\gamma^5-\frac{i}{\Lambda_U}\hat{\mathrm{k}}_1)(\hat{\mathrm{q}}_u+\mathrm{m}_\mu)\gamma^\alpha u(p_1,s_1), \quad (2.5)$$

$$M_{u(\mu^+\mu^-\to U_0\gamma)} = -\frac{ig}{4C_\mathrm{w}(q_u^2-m_\mu^2)}\frac{\lambda_0}{\Lambda_U^{d_u-1}}$$
$$\times\bar{v}(\mathrm{p}_2,\mathrm{s}_2)\gamma^\alpha(\mathrm{v}_\mu-\mathrm{a}_\mu\gamma_5)\varepsilon_\alpha^*(k_2)(\hat{\mathrm{q}}_u+\mathrm{m}_\mu)(1+i\gamma^5-\frac{i}{\Lambda_U}\hat{\mathrm{k}}_1)u(p_1,s_1). \quad (2.6)$$

From that, we calculate the square of the matrix and evaluate the DCS as a function of $\cos\theta$ and the CS as a function of $\sqrt{s}$ in the next section.

2.2. Numerical results and discussions

In the center of mass system, we can estimate the numerical values and evaluate the DCS and the CS from the following formula:

$$\frac{d\sigma}{d\Omega} = \frac{1}{64\pi^2 s}\frac{|\vec{k}_1|}{|\vec{p}_1|}|M|^2,\ d\Omega = d(\cos\theta)d\varphi. \quad (2.7)$$

To do that, we choose $\lambda_0 = 1,\ \lambda_1 = 1,\ \Lambda_U = 1TeV$ [5] and $\sqrt{s} = 14TeV$ [21] to evaluate the CS of the processes $\mu^+\mu^- \to U_0\gamma$ and $\mu^+\mu^- \to U_0 Z$ depending on d_U (Figures 2a and 2b) and the DCS as a function of $\cos\theta$ (Figures 3 and 4) and the CS depending on the center of mass energy $\sqrt{s}$ (Figures 5 and 6).

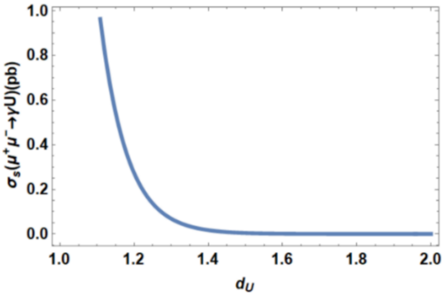

Figure 2a. The CS for $\mu^+\mu^- \to U_0\gamma$ as a function of d_U when the μ^+,μ^- beams are unpolarized

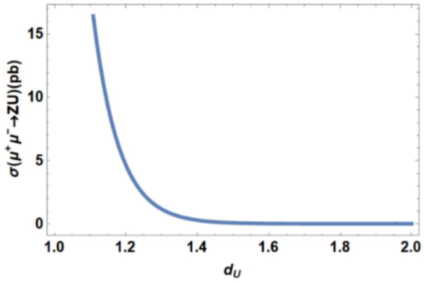

Figure 2b. The CS for $\mu^+\mu^- \to U_0 Z$ as a function of d_U when the μ^+,μ^- beams are unpolarized

According to Figures 2a and 2b, we can see that the CS of both processes reduces rapidly in the range of d_U from 1 to 1.3. We choose $d_U = 1.7$ for the next calculation because, in the range of d_U from 1.4 to 2, the CS does not depend on d_U. Furthermore, the CS of the process $\mu^+\mu^- \to U_0 Z$ is much larger than that of the process $\mu^+\mu^- \to U_0\gamma$ about $\sigma_s\left(\mu^+\mu^- \to U_0\gamma\right)/\sigma\left(\mu^+\mu^- \to U_0 Z\right) = 17$ times, which shows that the production in pair of U_0 with Z boson is better than that with photon from $\mu^+\mu^-$ collisions when the unpolarized μ^+,μ^-.

In the next step, we evaluate the dependence of the DCS on the cosine of the scattering angle θ on Figure 3 for the process $\mu^+\mu^- \to U_0\gamma$ and Figure 4 for the process. $\mu^+\mu^- \to U_0 Z$. Figures 3a, 3b, and 3c are the graphs of the DCS depending to $\cos\theta$ for the process $\mu^+\mu^- \to U_0\gamma$ according to the *s*-channel, the *t*-channel and the *u*-channel respectively. Figure 3d is for the case of mixing channels. According to the *s*-channel, most production particles are in the same direction as the incoming beams $(\theta = 0)$ or in the opposite direction to the incoming beams $(\theta = \pi)$. According to the *t*-channel, most production particles are in the same direction as the incoming beams $(\theta = 0)$ while according to the *u*-channel, this is the opposite direction, ie. the scattering angle $\theta = \pi$. In the case of mixing channels, the most production particles are analogous as the case for the *s*-channel and the largest value of the DCS is about 17×10^{-5} pb.

Figures 4a, 4b, and 4c are the graphs of the DCS depending to $\cos\theta$ for the process $\mu^+\mu^- \to U_0 Z$ according to the *s*-channel, the *t*-channel, and the *u*-channel respectively. Figure 4d is for the case of mixing channels. According to the *s*-channel, most production particles are in the same direction as the incoming beams $(\theta = 0)$ or in the opposite direction to the incoming beams $(\theta = \pi)$. According to the *t*-channel and the *u* - channel, most production particles are in the perpendicular direction to the direction of the incoming beams $(\theta = \pi/2)$. In the case of mixing channels, the most production particles are analogous to the case for the *t*-channel and *u* - channel and the maximum value of the DCS is about 2.5×10^{-2} pb.

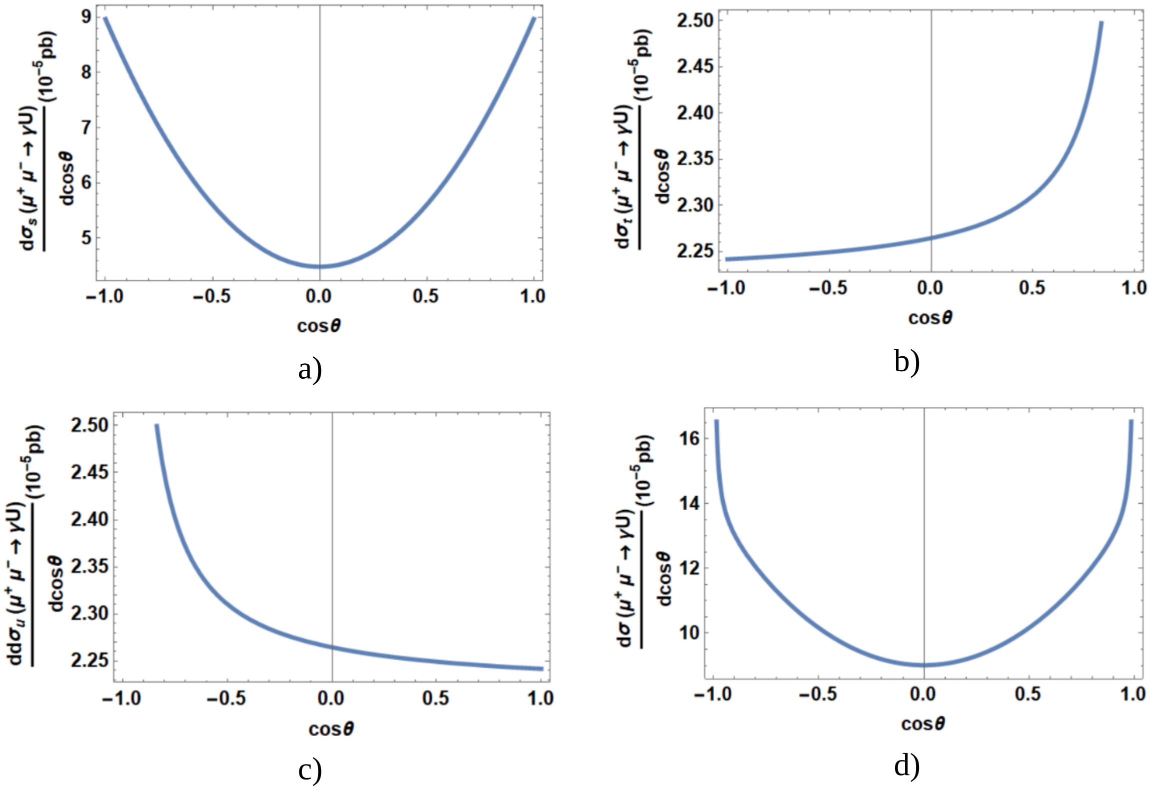

Figure 3. The DCS for $\mu^{+}\mu^{-} \to U_0\gamma$ ***as a function of*** $\cos\theta$

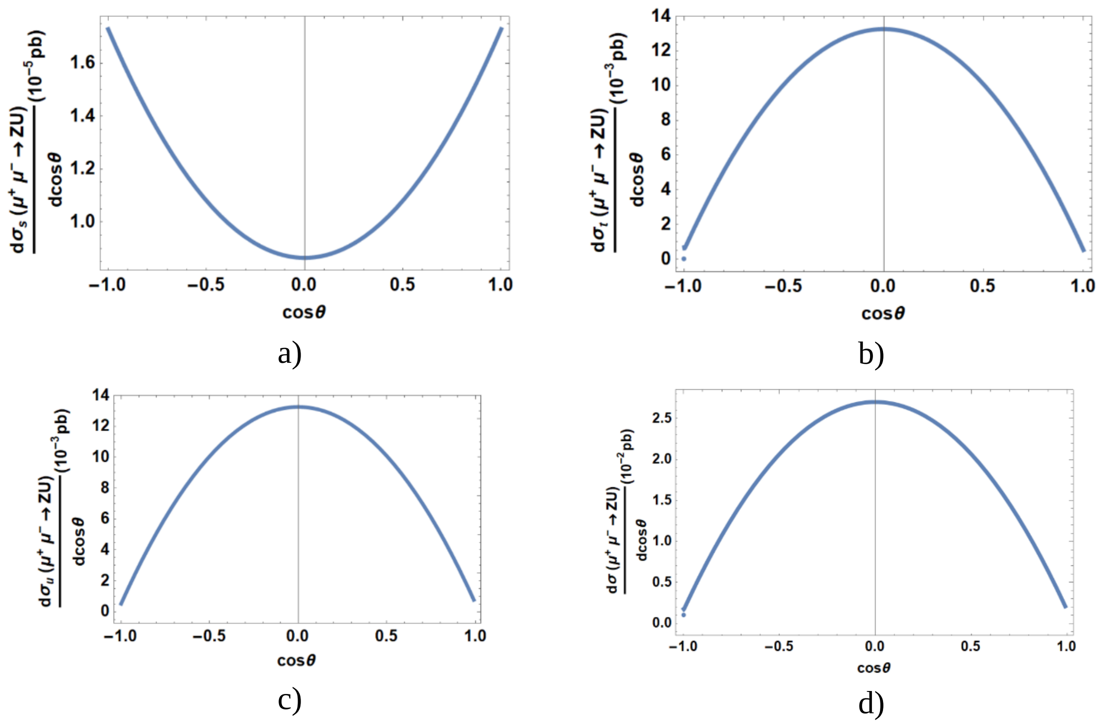

Figure 4. The DCS for $\mu^{+}\mu^{-} \to U_0 Z$ ***as a function of*** $\cos\theta$

In the final part, we study the dependence of the CS of the above collisions on the center of mass energy. Muon colliders give great potentials to produce the multi-TeV energy range. Therefore, we choose $\sqrt{s} = 14TeV$ because the energy of $14TeV$ would be sufficient to probe particles reaching the collider in the MAP. The dependence of CS on the $\sqrt{s} = 14TeV$ is shown in Figure 5 for the process $\mu^+\mu^- \to U_0\gamma$ and is shown in Figure 6 for the process $\mu^+\mu^- \to U_0 Z$.

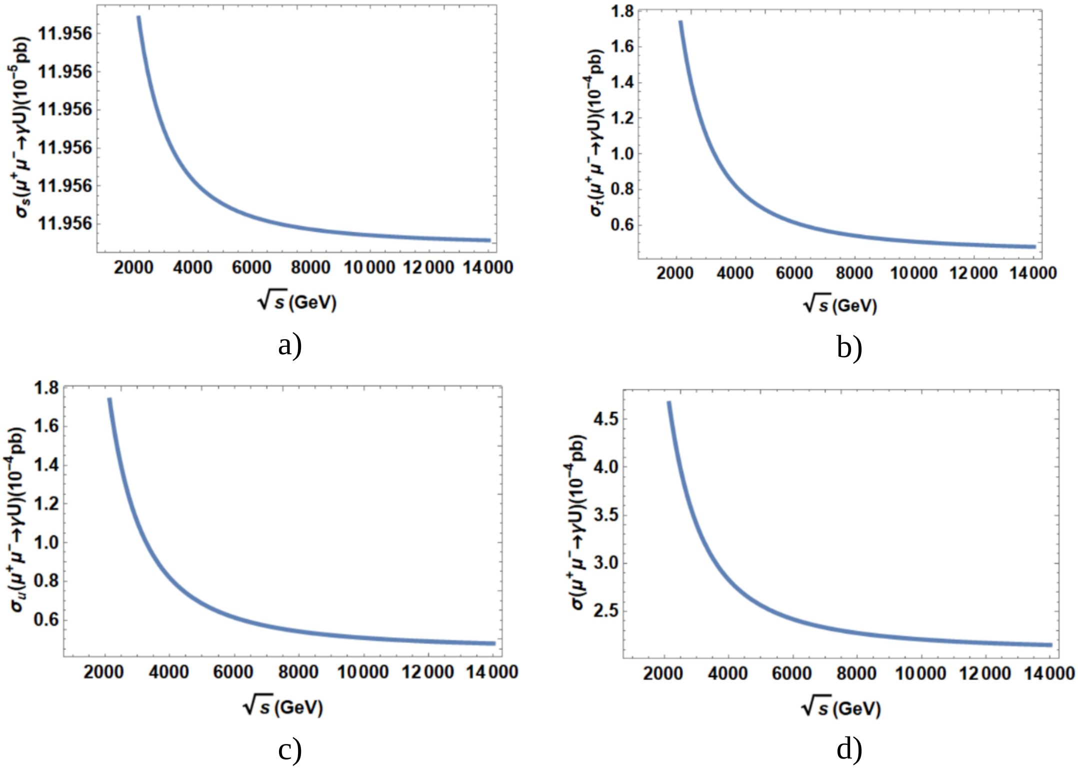

Figure 5. The dependence of the CS on the $\sqrt{s}$ for $\mu^+\mu^- \to U_0\gamma$

Figures 5a, 5b, and 5c are the graphs of the CS depending to $\sqrt{s}$ for the process $\mu^+\mu^- \to U_0\gamma$ according to the *s*-channel, the *t*-channel, and the *u*-channel respectively. Figure 5d is for the case of mixing channels. From these figures, we can see that the CS decreases quickly in the range of energy below 4000 GeV. This is a very advantageous range of energy for the MAP and the estimated values of the CS of the *t*-channel and the *u*-channel are the same and larger than that of the *s*-channel. In the case of mixing channels, the value of the CS is maximum (see Figure 5d). According to Figure 5d, the maximum value of the CS is about 5.0×10^{-4}pb. Similarly for the process $\mu^+\mu^- \to U_0 Z$, the CS of the *s*-channel decreases rapidly in the range of energy below $4000GeV$ (see Figure 6a) while for the *u*-channel, the *t*-channel and mixing channels (see Figures 6b, 6c, and 6d), the CS increases rapidly when the $\sqrt{s}$ increases. The CS of the *t*-channel and the CS of the *u*-channel are the same but the CS of mixing channels has the maximum value of about 4.0×10^{-2}pb (see Figure 6d).

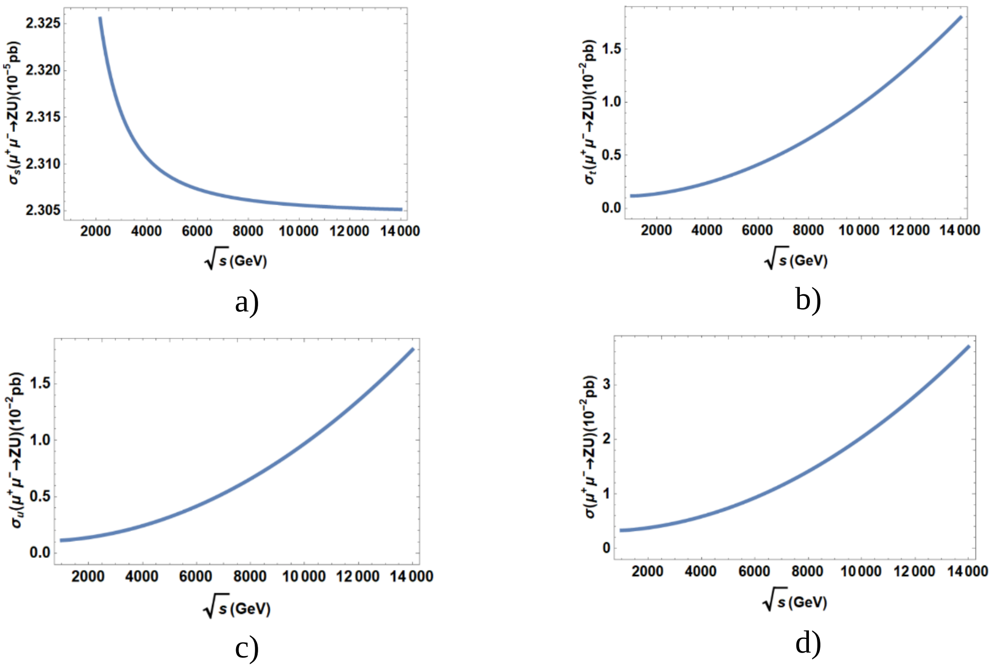

Figure 6. The dependence of the CS on the $\sqrt{s}$ ***for*** $\mu^+\mu^- \to U_0 Z$

Moreover, the CS of the process $\mu^+\mu^- \to U_0 Z$ is much larger than the CS of the process $\mu^+\mu^- \to U_0\gamma$ about $\sigma\left(\mu^+\mu^- \to U_0 Z\right)/\sigma\left(\mu^+\mu^- \to U_0\gamma\right) = 80$ times. Assuming a standard 10^7 operating seconds/year, the instantaneous luminosity $L = 3.3\times 10^{35}\,\mathrm{cm}^{-2}\mathrm{s}^{-1}$, and at $14TeV$ in the MAP [21], the number of events corresponding to the process $\mu^+\mu^- \to U_0 Z$ is

$$N = \sigma_{(\mu^+\mu^- \to U_0 Z)}\, L\, T = 13.2\times 10^4.$$

With hundreds of thousands of events, we can believe that the finding of unparticles signals through the production Z boson in the Standard Model at high energy levels is possible for the MAP project in LHC.

3. Conclusions

In the available range of energy at the high energy frontier muon collider in the MAP, the CS of both processes $\mu^+\mu^- \to U_0\gamma$ and $\mu^+\mu^- \to U_0 Z$ decreases rapidly in the range of d_U from 1 to 1.3. This expected result is consistent with the condition of d_U from 1 to 2 for scalar unparticles while in the range of d_U from 1.4 to 2, the CS does not depend on d_U. Especially, the CS of the process $\mu^+\mu^- \to U_0 Z$ is much larger than the CS of the process $\mu^+\mu^- \to U_0\gamma$ about 80 times. This means that the ability to search for the unparticles signals when products in pair with a Z boson is more optimistic than when products with the photon. Moreover, with hundreds of thousands of events, we can believe that the finding of scalar unparticles signals through the production Z boson in the Standard Model at high energy levels is possible for the MAP project in LHC.

In addition, from our obtained dependence of differential cross-section on the scattering angle, we can show the most favorable directions to obtain signals of scalar unparticles for processes $\mu^+\mu^- \to U_0\gamma$ and $\mu^+\mu^- \to U_0 Z$ For the process $\mu^+\mu^- \to U_0\gamma$, the most production particles are in the same direction as the incoming beams $(\theta = 0)$ or in the opposite direction to the incoming beams $(\theta = \pi)$ while for the process $\mu^+\mu^- \to U_0 Z$, the most production particles are in the perpendicular direction to the direction of the incoming beams $\left(\theta = \frac{\pi}{2}\right)$. These results may guide future experiments in searching for unparticles in muon collider.

REFERENCES

[1] H. Georgi, 2007. Unparticle Physics. *Phys. Rev. Lett.*, 98, 221601.

[2] H. Georgi, 2007. Another Odd Thing About Unparticle Physics. *Phys. Lett.*, B 650, pp. 275-278.

[3] T. Kikuchi, N. Okada, 2008. Unparticle physics and Higgs phenomenology. *Phys. Lett.*, B 661, pp. 360-364.

[4] G. Cacciapaglia, G. Marandella, and J. Terning, 2009. The AdS/CFT/Unparticle Correspondence. *JHEP* 02(2009)049, arXiv:0804.0424, doi:10.1088/1126-6708/2009/02/049.

[5] K. Cheung, W.Y. Keung and T. C. Yuan, 2007. Collider Phenomenology of Unparticle Physics. *Phys. Rev.*, D 76, 055002.2.

[6] H. Davoudiasl, 2007. Constraining unparticle Physics with cosmology and astrophysics. *Phys. Rev. Lett.*, 99, 141301.

[7] J. R. Mureika, 2008. Unparticle-enhanced black holes at the LHC. *Phys. Lett.*, B 660, pp. 561-566.

[8] J. R. Mureika, 2009. Differentiating unparticles from extra dimensions via mini black hole thermodynamics. *Phys. Rev.*, D 79, 056002.2.

[9] J. R. Mureika and E. Spallucci, 2010. Vector unparticle enhanced black holes: Exact solutions and thermodynamics. *Phys. Lett.*, B 693, pp. 129-132.2.

[10] J. P. F. LeBlanc and A. G. Grushin, 2015. Unparticle mediated superconductivity. *New J. Phys.*, 17, 033039.

[11] P. W. Phillips, B. W. Langley, J. A. Hutasoit, 2012.2. Un-Fermi Liquids: Unparticles in Strongly Correlated Electron Matter. *Phys. Rev.*, B 88, 115129.

[12] K. Limtragool, P. Phillips, 2015. Power-law Optical Conductivity from Unparticles: Application to the Cuprates. *Phys. Rev.*, B 92, 155128.

[13] CMS Collaboration, 2015. Search for dark matter, extra dimensions, and unparticles in monojet events in proton-proton collisions at $\sqrt{s} = 8TeV$. *Eur. Phys. J.*, C 75, 235.

[14] V. Khachatryan and *et al*., 2016. Search for dark matter and unparticles produced in association with a Z boson in proton - proton collisions at $\sqrt{s} = 8TeV$ at CMS. *Phys. Rev*., D 92, 2, 052011.

[15] CMS Collaboration, 2017. Search for dark matter and unparticles in events with a Z boson and missing transverse momentum in proton-proton collisions at $\sqrt{s} = 13TeV$. *JHEP* 02.2. 061, [arxiv: 1701.02042].

[16] T.M. Aliev, S. Bilmis, M. Solmaz, and I. Turan, 2017. *Scalar Unparticle Signals at the LHC. Phys. Rev*., D 95, 095005.

[17] N.T. Hau and D.T.L. Thuy, 2019. Higgs and vector unparticle production via $\mu^+\mu^-$ collision in the Randall-Sundrum model. *VNU Journal of Science: Math-Phys.*, Vol. 35, No. 4, pp. 93-98.

[18] L.N.Thuc and D.T.L. Thuy, 2020. The scalar unparticle production from the collision process γe^- in the Unparticle Physics. *VNU Journal of Science: Math-Phys*., Vol. 36, No. 1, pp. 7-12.

[19] N.T. Hau and D.T.L. Thuy, 2019. The process $e^+e^- \to \phi U$ via vector unparticle exchange in the Randall-Sundrum model. *HNUE Journal of Science*, Vol. 64, No. 6, pp. 39-44.

[20] R. B. Palmer, 2014. Muon Colliders. *Reviews of Accelerator Sci and Tech.*, Vol. 7, pp. 137-159, DOI: 10.1142/S1793626814300072.

[21] D.Neuffer and V.Shiltsev, 2018. On the feasibility of a pulsed 14TeV c.m.e. muon collider in the LHC tunnel. *JINST*, 12.2. T10002.2.